

Non-comoving baryons and cold dark matter in cosmic voids

Ismael Delgado Gaspar^{a,1}, Juan Carlos Hidalgo^{b,1}, Roberto A. Sussman^{c,2}

¹Instituto de Ciencias Físicas, Universidad Nacional Autónoma de México, A.P. 48–3, 62251 Cuernavaca, Morelos, México.

²Instituto de Ciencias Nucleares, Universidad Nacional Autónoma de México, A. P. 70–543, 04510 Ciudad de México, México.

Received: date / Accepted: date

Abstract We examine the fully relativistic evolution of cosmic voids constituted by baryons and cold dark matter (CDM), represented by two non-comoving dust sources in a Λ CDM background. For this purpose, we consider numerical solutions of Einstein’s field equations in a fluid–flow representation adapted to spherical symmetry and multiple components. We present a simple example that explores the frame-dependence of the local expansion and the Hubble flow for this mixture of two dusts, revealing that the relative velocity between the sources yields a significantly different evolution in comparison with that of the two sources in a common 4-velocity (which reduces to a Lemaître–Tolman–Bondi model). In particular, significant modifications arise for the density contrast depth and void size, as well as in the amplitude of the surrounding over-densities. We show that an adequate model of a frame-dependent evolution that incorporates initial conditions from peculiar velocities and large-scale density contrast observations may contribute to understand the discrepancy between the local value of H_0 and that inferred from the CMB.

Keywords Large-scale structure · Voids formation · Cosmology · Classical general relativity

1 Introduction

The generic term “Cosmic Voids” denotes $\sim 10 - 120$ Mpc sized round shaped low density regions surrounded by over-dense filaments and walls, all of which conform the “cosmic web” of large-scale structure (baryons and CDM) revealed by observations and N-body simulations [1]. There is a large body of literature on cosmic voids, from seminal early work

[2, 3] to recent extensive reviews [4–7] and detailed catalogues (see a summary in [8]). As revealed by these reviews and references therein: (i) cosmic voids enclose only 15% of cosmic matter–energy (within the Λ CDM paradigm) but constitute about 77% of cosmic volume; (ii) they form from early negative density contrast perturbations; (iii) they roughly keep their rounded shape and (iv) their dynamics is relatively insensitive to considerations from baryon physics. This relatively simple and pristine dynamics renders them as ideal structure systems to improve the theoretical modeling of generic cosmological observations [9–11], and to assess several open problems in cosmology: the nature of dark matter and dark energy [12–21], redshift space distortions [22–25], Cosmic Microwave Background (CMB) properties [26–30], Baryonic Acoustic Oscillations (BAO) [31], alternative gravity theories [32–37], local group kinematics and peculiar velocity fields [38–44], as well as theoretical issues such as gravitational entropy [45, 46].

The usual approach to study the nature and dynamics of cosmic voids is through Newtonian gravity [47] (see reviews [4–7] and references cited therein for examples of studies based on analytic work, perturbations and N-body simulations). These studies have put forward various forms of “universal” density profiles [48, 49] that fit observations and catalogues. However, given the fact that cosmic voids are approximately spherical structures that tend to become more spherical as they evolve (see [50] for the first proof of this fact known as the “*bubble theorem*”¹ and also [4–7, 51–53] for further discussions and comparison with N-body simulations), it is also feasible to study them by means of spherically symmetric, exact and numerical solutions of Einstein’s equations. As examples of analytic and semi-analytic general relativistic studies, there are many based on Lemaître–

^ae-mail: ismaeldg@icf.unam.mx

^be-mail: hidalgo@icf.unam.mx

^ce-mail: sussman@nucleares.unam.mx

¹ The “Bubble Theorem” states that an isolated underdensity (void) tends to evolve into a spherical shape, explicitly: “*as the void becomes bigger, its asphericities will tend to disappear*” [50].

Tolman–Bondi (LTB) dust models [54–57], or the more general non–spherical (but quasi–spherical) Szekeres models [58–61]. While numerical relativity techniques have already been applied in a cosmological context beyond spherical symmetry [62–67], most relativistic numerical studies on cosmic voids still rely on metric–based techniques involving the Misner–Sharp mass function, and thus their validity is restricted to spherical symmetry [68–71]. In particular, four relevant studies that specifically examine general relativistic void dynamics for spherical symmetry preceding our study are [72–75].

In the present article we examine the fully general relativistic evolution of a spherically symmetric cosmic void, assuming as matter source a mixture of non–interactive baryons and CDM species, each evolving along a different 4–velocity. Specifically, we consider the evolution of a generic cosmic void suitably embedded in a Λ CDM background. Since CDM is the dominant clustering source, we assume a frame in which its 4–velocity is comoving, whereas the baryons evolve along a non–comoving 4–velocity that defines a non–trivial field of spacelike relative velocities with respect to the CDM frame. Consequently the 4–velocities of the two dust sources are related by a boost, and the energy–momentum tensor of the mixture (as described in the comoving frame) no longer has the form of a perfect fluid, but that of a complicated “fluid” energy–momentum tensor that contains effective pressures and energy flux terms associated with the relative velocity field.

In order to deal with the general relativistic dynamics for this energy–momentum tensor, we do not resort to the traditional metric based methods of [72–75], but consider the system of first order partial differential equations (PDEs) provided by the “fluid–flow” (or “1+3”) representation of Einstein’s equations [76–78] in terms of evolution equations and constraints for the covariant quantities associated with the CDM comoving 4–velocity. These covariant variables are (i) kinematic: expansion scalar, 4–acceleration, shear tensor and relative velocity, all computed from the CDM frame; (ii) source terms: the total energy density, pressure and energy flux that arise from the relative velocity and (iii) the electric Weyl tensor. These equations (evolutions and constraints) must be supplemented by spacelike constraints.

The plan of the paper is as follows. In Section 2, we introduce a model for the evolution of a generic mixture of fluids in a spherically symmetric spacetime. This model is specialized to the case of two non–interacting dust–like fluids, namely CDM and baryons, in Section 3. We examine the numerical solutions of the resulting system of partial differential equations (PDEs) in a void formation scenario. Through representative numerical examples, we look at the influence of the relative baryon–CDM velocity on the evolution and present–day final structure. Our results are summarized and discussed in Section 4. Finally, we have included

three appendices that complement the main text. Appendix A provides the general tensorial evolution equations of the 1 + 3 description; while in Appendix B and Appendix C, we present the dimensionless baryon–CDM system of PDEs and show its (single–fluid) LTB limit.

2 A mixture of multiple fluids in spherical symmetry

A spherically symmetric spacetime is characterized by the line element,

$$ds^2 = g_{\mu\nu} dx^\mu dx^\nu = -N^2 dt^2 + B^2 dr^2 + Y^2 (d\theta^2 + \sin^2(\theta) d\phi^2), \quad (1)$$

where the metric coefficients N , B and Y are functions of the radial and time coordinates. Notice that this metric contains as a particular case the Robertson–Walker line element, a solution recovered in our examples at scales larger than ~ 100 Mpc at $z = 0$.

Regarding the evolution of a mixture of non–comoving fluids, the fluid elements of each species will evidently present its own 4–velocity. In absence of specific criteria, a useful choice of “reference frame” is the one of the dominant species². Hence the family of fundamental observers will evolve with comoving 4–velocity,

$$u^\mu = \frac{1}{N} \delta_t^\mu, \quad (2)$$

which defines the convective fluid–flow (or time derivative) and space–like gradients (orthogonal to u^μ):

$$\dot{X} = u^\mu \nabla_\mu X = \frac{X_{,t}}{N} \quad \text{and} \quad \tilde{\nabla}_\mu X = h^\nu_\mu \nabla_\nu X. \quad (3)$$

The kinematic parameters associated with a spherically symmetric fluid as measured by the fundamental observers are the expansion scalar, 4–acceleration and shear tensor (the vorticity vanishes identically):

$$H = \frac{\Theta}{3} = \frac{1}{3} \tilde{\nabla}_\mu u^\mu, \quad (4a)$$

$$\dot{u}_\mu = u^\nu \nabla_\nu u_\mu, \quad (4b)$$

$$\sigma_{\mu\nu} = \tilde{\nabla}_{(\mu} u_{\nu)} - \dot{u}_\mu u_\nu - H h_{\mu\nu}. \quad (4c)$$

The Einstein field equations can be recast [76–78] as a first order system of “1 + 3” evolution and constraint equations involving these kinematic parameters, together with the energy density ρ , isotropic p and anisotropic pressure $\pi_{\mu\nu}$ and energy flux q_μ of the source given by the energy–momentum tensor, as well as the electric Weyl tensor $E_{\mu\nu} = C_{\mu\alpha\nu\beta} u^\alpha u^\beta$ (the magnetic Weyl tensor identically vanishes). This system (displayed in Appendix A) is ideal for a numerical treatment in which all variables have a clear physical and geometric

²This choice, however, is arbitrary and one could also choose the fundamental observers moving with the baryon component or even a frame in which the total momentum flux density vanishes $q^\mu = 0$.

meaning. Since it is based on a 4-velocity flow it is fully covariant, and thus it is readily applicable to spacetimes that are not spherically symmetric.

For the spherically symmetric metric (1) we have

$$H = \frac{1}{3} \left(\frac{2\dot{Y}}{Y} + \frac{\dot{B}}{B} \right), \quad \dot{u}_\mu = \tilde{\nabla}_\mu (\ln N) = A \delta_\mu^r, \quad A \equiv \frac{N_r}{N}, \quad (5)$$

and the space-like symmetric trace-free tensors σ_ν^μ and E_ν^μ can be written as

$$\sigma_\nu^\mu = \Sigma e_\nu^\mu, \quad E_\nu^\mu = W e_\nu^\mu. \quad (6)$$

Here W and Σ are scalar functions,

$$\Sigma = \frac{1}{3} \left(\frac{\dot{Y}}{Y} - \frac{\dot{B}}{B} \right), \quad W = -\Psi_2, \quad (7)$$

with Ψ_2 the conformal invariant of Petrov type D spacetimes, and $e_\nu^\mu = h_\nu^\mu - 3n^\mu n_\nu = \text{Diag}[0, -2, 1, 1]$ is the tensor basis that serves as eigenframe for spacelike symmetric trace free tensors in Petrov type D spacetimes, with $h_{\mu\nu} = g_{\mu\nu} + u_\mu u_\nu$ and $n_\mu = \sqrt{g_{rr}} \delta_\mu^r$ the projection tensor and a spacelike normal vector tangent to the orbits of $\text{SO}(3)$ (note that $\dot{e}_\nu^\mu = 0$).

The 4-velocity of the other non-comoving components are related to u^μ via the relative velocity measured by the fundamental observers $v_{(i)}^\mu$, defined such that $v_{(i)}^\mu u_\mu = 0$. Then, the 4-velocity of the i -th fluid reads,

$$u_{(i)}^\mu = \gamma_{(i)} \left(u^\mu + v_{(i)}^\mu \right), \quad \text{with} \quad \gamma_{(i)} = \left(1 - v_{(i)}^2 \right)^{-\frac{1}{2}}, \quad (8)$$

where “ i ” labels the components and $v_{(i)}^2 = g_{\mu\nu} v_{(i)}^\mu v_{(i)}^\nu$.

The total energy-momentum tensor is made up of all the contributions from the different species, and in general it will no longer be the energy-momentum tensor of a perfect fluid, but

$$T^{\mu\nu} = \sum_i T_{(i)}^{\mu\nu} = \rho u^\mu u^\nu + p h^{\mu\nu} + 2q^{(\mu} u^{\nu)} + \pi^{\mu\nu}, \quad (9)$$

where ρ , p , $\pi^{\mu\nu}$ and q^μ are the energy density, isotropic and anisotropic pressures³, and the energy flow measured by the fundamental observers along u^μ . These components are determined by projecting the energy-momentum tensor parallel and orthogonal to u^μ [78, 79]:

$$\rho = T^{\mu\nu} u_\mu u_\nu, \quad q^\mu = -T^{\mu\nu} u_\nu - \rho u^\mu, \quad p = \frac{1}{3} T^{\mu\nu} h_{\mu\nu}, \quad (10a)$$

$$\pi_{\mu\nu} = T_{\langle\mu\nu\rangle} = \left[h_{(\mu}^\eta h_{\nu)}^\nu - \frac{1}{3} h_{\mu\nu} h^{\eta\nu} \right] T_{\eta\nu}. \quad (10b)$$

³ In this setup, the cosmological constant is implicitly considered by the substitution $\rho \rightarrow \rho + \Lambda$ and $p \rightarrow p - \Lambda$.

Although the total energy-momentum tensor is always conserved, the energy-momentum tensors of the individual components are not necessarily conserved. If there are non-gravitational interactions between them, they satisfy $\nabla_\nu T_{(i)}^{\mu\nu} = J_{(i)}^\mu$, where $J_{(i)}^\mu$ is the rate of energy and momentum densities transfer between species i as measured in the u^μ -frame. In absence of non-gravitational interaction these energy-momentum tensors are separately conserved: $J_{(i)}^\mu = 0$ for all i .

2.1 A mixture of non-interacting perfect fluids

We now focus on the case of a mixture of non-interacting fluids, each one a perfect fluid with a suitable equation of state in its intrinsic frame (denoted with $*$):

$$p_{(i)}^* = w_{(i)} \rho_{(i)}^*, \quad \text{in general} \quad w_{(i)} = w_{(i)}(t, r). \quad (11)$$

In this way, the total energy-momentum tensor follows from adding up the corresponding tensors of the dynamically significant species as seen from the u^μ frame (eqs. (9) and (10)).

Explicitly, if we choose the fundamental observers those along $u_{(0)}^\mu$, then the contribution to the total energy-momentum tensor of the “0” component reads

$$T_0^{\mu\nu} = \rho_0^* u^\mu u^\nu + p_0^* h^{\mu\nu}. \quad (12)$$

On the other hand, the energy-momentum tensor of the i -th component comoving with velocity $u_{(i)}^\mu$ (see eq. (8)) takes the form

$$T_{(i)}^{\mu\nu} = \rho_{(i)} u^\mu u^\nu + p_{(i)} h^{\mu\nu} + 2q_{(i)}^{(\mu} u^{\nu)} + \pi_{(i)}^{\mu\nu}, \quad (13)$$

with the dynamical quantities given by [78, 79]:

$$\rho = \sum_i \rho_{(i)}, \quad \rho_{(i)} = \gamma_{(i)}^2 (1 + w_{(i)} v_{(i)}^2) \rho_{(i)}^*, \quad (14a)$$

$$p = \sum_i p_{(i)}, \quad p_{(i)} = \left[w_{(i)} + \frac{1}{3} \gamma_{(i)}^2 v_{(i)}^2 (1 + w_{(i)}) \right] \rho_{(i)}^*, \quad (14b)$$

$$q^\mu = \sum_i q_{(i)}^\mu, \quad q_{(i)}^\mu = \gamma_{(i)}^2 (1 + w_{(i)}) \rho_{(i)}^* v_{(i)}^\mu, \quad (14c)$$

$$\pi^{\mu\nu} = \sum_i \pi_{(i)}^{\mu\nu}, \quad \pi_{(i)}^{\mu\nu} = \gamma_{(i)}^2 (1 + w_{(i)}) \rho_{(i)}^* v_{(i)}^{\langle\mu} v_{(i)}^{\nu\rangle}, \quad (14d)$$

where for spherical symmetry spacetimes the anisotropy tensor can be written as $\pi_{(i)\nu}^\mu = \Pi_{(i)} e_\nu^\mu$, with $\Pi_{(i)}$ to be determined from Eq. (14d).

The dynamics of this fluid mixture can be determined from the first order “1 + 3” fluid flow representation of Einstein’s field equations given in Appendix A, by direct substitution of ρ , p , $\pi_{\mu\nu}$, q_μ by (14a)–(14d), with

$$q_{(i)\mu} = Q_{(i)} \delta_\mu^r, \quad v_{(i)\mu} = V_{(i)} \delta_\mu^r, \quad (15)$$

and $\dot{u}_\mu, \sigma_{\mu\nu}, E_{\mu\nu}$ obtained from (5) and (7). For spherical symmetry this system can be further simplified and complemented by evolution equations for the metric functions Y, B and $\chi \equiv Y'$ that can be obtained from (5) and (7). Since each one of the proper tensors $\dot{u}_\mu, \sigma_{\mu\nu}, E_{\mu\nu}$ is fully determined by a single scalar function A, Σ, W , the tensorial system in Appendix A becomes a dynamical system involving only scalar functions:

$$\dot{Y} = Y(H + \Sigma), \quad (16a)$$

$$\dot{\chi} = A(\Sigma + H)Y - 2\chi\Sigma + \chi H + \frac{1}{2}\kappa QY, \quad (16b)$$

$$\dot{B} = B(H - 2\Sigma), \quad (16c)$$

$$\begin{aligned} \dot{H} = & -H^2 - 2\Sigma^2 - \frac{1}{6}\kappa(\rho + 3p) + \frac{1}{3}\frac{A^2}{B^2} + \frac{1}{3}\frac{A_{,r}}{B^2} \\ & - \frac{1}{3}\frac{AB_{,r}}{B^3} + \frac{2}{3}\frac{A\chi}{B^2Y}, \end{aligned} \quad (16d)$$

$$\begin{aligned} \dot{\Sigma} = & \Sigma^2 - 2H\Sigma + \frac{1}{2}\kappa\Pi - W - \frac{1}{3}\frac{A^2}{B^2} + \frac{1}{3}\frac{A\chi}{B^2Y} \\ & + \frac{1}{3}\frac{AB_{,r}}{B^3} - \frac{1}{3}\frac{A_{,r}}{B^2}, \end{aligned} \quad (16e)$$

$$\begin{aligned} \dot{W} + \frac{1}{2}\kappa\dot{\Pi} = & -3(H + \Sigma)W - \frac{1}{2}\kappa(\rho + p)\Sigma \\ & - \frac{1}{2}\kappa(H - \Sigma)\Pi - \kappa\frac{QB_{,r}}{6B^3} + \kappa\frac{Q_{,r}}{6B^2} - \kappa\frac{Q\chi}{6B^2Y} + \kappa\frac{AQ}{3B^2}, \end{aligned} \quad (16f)$$

where A is defined in (5), $Q = \sum_i Q_{(i)}$ and $\Pi = \sum_i \Pi_{(i)}$. This system must be complemented by the following constraints:

$$W = -\frac{1}{6}\kappa\rho - \frac{\kappa}{2}\Pi + \frac{M}{Y^3}, \quad (17a)$$

$$N_{,r} = AN, \quad (17b)$$

$$H^2 = \frac{1}{3}\kappa\rho - \mathcal{K} + \Sigma^2. \quad (17c)$$

Here \mathcal{K} is the spatial curvature:

$$\mathcal{K} \equiv \frac{{}^{(3)}\mathcal{R}}{6} = \frac{(KY)_{,r}}{3Y^2\chi}, \quad \text{with } K = 1 - \frac{\chi^2}{B^2}, \quad (18)$$

and M is the Misner–Sharp function

$$M = \frac{Y}{2} \left[\dot{Y}^2 - \frac{\chi^2}{B^2} + 1 \right] = \frac{Y}{2} \left[Y^2(H + \Sigma)^2 - \frac{\chi^2}{B^2} + 1 \right], \quad (19)$$

that is characteristic of spherically symmetric spacetimes. Notice that this function furnishes an expression for W through the constraint (17a) that allows us to eliminate the evolution equation (16f) for \dot{W} (and W in (16e)), though, since M is fully expressible through (19) in terms of the variables of (16), we do not need to use this function explicitly to integrate this system (we just eliminate M with (19))⁴. Besides

⁴ To work beyond spherical symmetry we can easily do away with the usage of the Misner–Sharp mass function and work with the electric and/or magnetic Weyl tensor.

these constraints, we also need to supplement the system with the conservation equation for each fluid:

$$\dot{\rho}_0 = -3(\rho_0^* + p_0^*)H, \quad A = -\frac{p_{0,r}^*}{\rho_0^* + p_0^*}, \quad (20a)$$

$$\begin{aligned} \dot{\rho}_{(i)} = & -3(\rho_{(i)} + p_{(i)})H - 2\frac{AQ_{(i)}}{B^2} - 6\Pi_{(i)}\Sigma - 2\frac{Q_{(i)}\chi}{YB^2} \\ & - \frac{Q_{(i),r}}{B^2} + \frac{Q_{(i)}B_{,r}}{B^3}, \end{aligned} \quad (20b)$$

$$\begin{aligned} \dot{Q}_{(i)} = & -3HQ_{(i)} - p_{(i),r} - A\rho_{(i)} - Ap_{(i)} + 2\Pi_{(i)}A + 2\Pi_{(i),r} \\ & + \frac{6\Pi_{(i)}\chi}{Y}. \end{aligned} \quad (20c)$$

Finally, the radial component velocity $V_{(i)}$ of the i -th fluid in (15) can be determined algebraically from (14a) and (14c).

3 Void evolution from a mixture of two decoupled dusts

The main characteristic of cosmic voids is the underdensity profile that depends on the (roughly) radial distance on Mpc scales. However, the usual single fluid (dust) approach generally focuses on the void dimensions (size and the depth of the density contrast) and the value of the local expansion [80], while the relative velocity between the dynamically significant species is usually ignored. In this section we show that the multiple components scenario brings important modifications to the evolution of cosmic voids.

3.1 A numerical example of the two–component mixture

To stress the above it is illustrative to look at the case of a mixture of two dust fluids identified as CDM and baryonic matter, including a cosmological constant characterized by the present–day parameters from Planck 2015 [81], in order to accommodate a Λ CDM asymptotic background model. We consider the fundamental observers comoving with dark matter $u_{\text{DM}}^\mu = \delta_i^\mu$; consequently, the baryonic matter will have 4–velocity,

$$u_{\text{B}}^\mu = \gamma(u_{\text{DM}}^\mu + v^\mu), \quad \text{with } \gamma = (1 - v^2)^{-\frac{1}{2}}, \quad \text{and } v_\mu = V\delta_\mu^r, \quad (21)$$

and the energy–momentum tensor, eq. (9), will be the sum of the CDM and baryonic components:

$$T^{\mu\nu} = T_{\text{DM}}^{\mu\nu} + T_{\text{B}}^{\mu\nu} = \rho u^\mu u^\nu + p h^{\mu\nu} + 2q^{(\mu} u^{\nu)} + \pi^{\mu\nu}, \quad (22a)$$

with

$$T_{\text{DM}}^{\mu\nu} = \rho_{\text{DM}} u^\mu u^\nu \quad \text{and} \quad T_{\text{B}}^{\mu\nu} = \rho_{\text{B}} u^\mu u^\nu + p_{\text{B}} h^{\mu\nu} + 2q_{\text{B}}^{(\mu} u^{\nu)} + \pi_{\text{B}}^{\mu\nu}, \quad (22b)$$

such that one can identify the following quantities (as defined in (14) and (15)),

$$\rho = \rho_{\text{DM}} + \rho_{\text{B}}, \quad p \equiv p_{\text{B}} = \frac{1}{3} \gamma^2 v^2 \rho_{\text{B}}^*, \quad (22c)$$

$$Q \equiv Q_{\text{B}} = \gamma^2 \rho_{\text{B}}^* V, \quad \Pi \equiv \Pi_{\text{B}} = \frac{1}{3} \gamma^2 \rho_{\text{B}}^* v^2, \quad (22d)$$

$$\rho_{\text{DM}} \equiv \rho_{\text{DM}}^*, \quad \rho_{\text{B}} = \gamma^2 \rho_{\text{B}}^*. \quad (22e)$$

Note that the pressure, heat flow and anisotropic stress terms are zero when $V = 0$ (CDM and baryons with common 4-velocity: LTB limit). Consequently, the evolution will be governed by the system of equations that results from substituting $0 \rightarrow \text{DM}$ and $i \rightarrow \text{B}$ in eq. (16) and considering the energy-momentum tensor variables (22). The resulting dimensionless system of equations is presented explicitly in Appendix B.

We examine the numerical solutions of this two-dust system in a grid simulating a cosmic void of present-day radius ~ 60 Mpc. Starting from linear initial conditions at $z = 23$ we follow its evolution until $z = 0$ (see below for the justification of this choice of initial redshift). The initial CDM density, spatial curvature, and the relative velocity profiles are taken as Gaussian functions of linear amplitude with respect to the background parameters. In all our simulations the baryonic density is initially homogeneous and equal to its value in the background (as seen in its intrinsic frame),

$$\left[\frac{8\pi \rho_{\text{DM}}}{3 H^2} \right]_{\text{ini}} = \Omega_{\text{DM}}^{\text{ini}} - \mu_c \exp\left(-\frac{\xi}{\sigma_\mu}\right)^2, \quad (23a)$$

$$[K]_{\text{ini}} = -k_c \xi^2 \exp\left(-\frac{\xi}{\sigma_K}\right)^2, \quad (23b)$$

$$[V]_{\text{ini}} = V_c \xi^2 \exp\left(-\frac{\xi}{\sigma_v}\right)^2. \quad (23c)$$

In the expressions above $\mu_c \sim 0.01$, $k_c \sim 0.05$, $\sigma_K = \sigma_\mu = 0.03$, $\sigma_v = 0.025$, and $r = l_* \xi$. From this, the spatial curvature (\mathcal{K}) is derived from Eqs. (18) and (23b). The characteristic length is $l_* \sim 60$ Mpc, while the characteristic speed constant V_c (and the maximum of the velocity V_{peak}) will be specified further below. Figure 1 shows the typical initial profiles used for the numerical analysis.

3.2 Evolution of density profiles

To look at the effect of the relative velocity on voids and wall formation we develop a code capable of handling test cases with given initial densities for each species, a given curvature profile, and a series of profiles for the relative velocity (V_{peak}).

In Fig. 2 we display the baryon and CDM density contrasts at $z = 0$ for different initial velocity profiles. As a reference, we have included the case in which both baryons and

CDM are comoving (LTB solution). We find that even non-relativistic relative velocity values exert non-trivial effects on present-day configurations as density contrasts become non-linear. On the other hand, the void size depends on the sign of V , so that smaller voids result from initially negative values for the relative velocity. We also illustrate the evolution of the density contrast profiles for the specific case of $V_{\text{peak}} \sim 7 \times 10^{-3}$ (corresponding to the red curves in Fig. 2), snapshots for different values of z are displayed in Fig. 3.

Notice that as the evolution proceeds the density contrast at the surrounding wall increases, reaching probably a shell-crossing singularity. We interpret this as the onset of an intricate virialization process, a stage of structure formation that marks the limit of validity of the dust model, and that lies beyond the scope of this work (discussed elsewhere in the literature [83, 84]). Since our purpose is to look at the simultaneous evolution of the matter-energy components (CDM and baryons) within the void before the onset of virialization, we have chosen $z = 23$ as the initial time slice, simply because it is easier to set the initial conditions at this time than at, say, the linear regime of the last scattering time $z \simeq 1100$, well before gravitational clustering becomes dynamically significant. However, these initial conditions are idealized but not fine-tuned or unrealistic, they simply correspond to a spherically symmetric realization of the generic spectrum of random CDM and baryon perturbations, characteristic of the linear regime at the last scattering surface $z \simeq 1100$, which evolve to produce a void of the desired size.

3.3 Local expansion of the components

Let us now focus on the effects of a relative velocity in the measure of kinematic quantities. In the case of a single fluid, the comoving observers define a natural threading of the spacetime by the future-directed unit timelike vector field u^μ . In our case, as we stressed before, the choice of the fundamental observers is not unique, and observers comoving with each fluid will measure the kinematic quantities with different magnitudes. In fact, due to a change of frame, the local expansion of CDM ($H_{\text{DM}} \equiv H$ in this frame) will depart from the expansion of the baryonic matter H_{B} , which is given by

$$3H_{\text{B}} = \Theta_{\text{B}} = h_{\text{B}\mu}^{\nu} \nabla_{\nu} u_{\text{B}}^{\mu}, \quad (24)$$

where $h_{\text{B}}^{\mu\nu} = u_{\text{B}}^{\mu} u_{\text{B}}^{\nu} + g^{\mu\nu}$ is the projection tensor and u_{B}^{μ} is the 4-velocity of the baryonic matter given in eq. (21). We find by computing (24) a relation between both estimations of the expansion,

$$\begin{aligned} 3H_{\text{B}} &= \left[\left(\frac{2Y_{,r}}{Y} - \frac{B_{,r}}{B} \right) \frac{V}{B^2} + \frac{V_{,r}}{B^2} + 3H_{\text{DM}} \right] \gamma + \frac{V}{B^2} \gamma_{,r} + \dot{\gamma}, \\ &\simeq \left(\frac{2\mathcal{K}}{Y} - \frac{B_{,r}}{B} \right) \frac{V}{B^2} + \frac{V_{,r}}{B^2} + 3H_{\text{DM}} + V\dot{V}, \end{aligned} \quad (25)$$

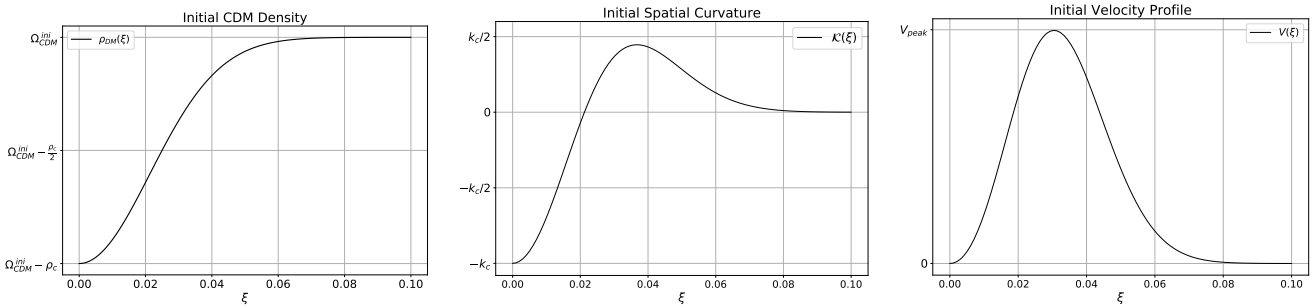


Fig. 1 Initial CDM density, spatial curvature and baryon relative velocity profiles as functions of $\xi = r/l_*$. The initial functions are taken as Gaussian perturbations to the background functions, given by eq. (23) with $\mu_c \sim 0.01$, $k_c \sim 0.05$, $\sigma_K = \sigma_\mu = 0.03$, $\sigma_v = 0.025$, while V_{peak} is varied over values between -10^{-3} and $\sim 10^{-2}$. The initial baryon matter density is homogeneous, as seen from the baryons intrinsic frame.

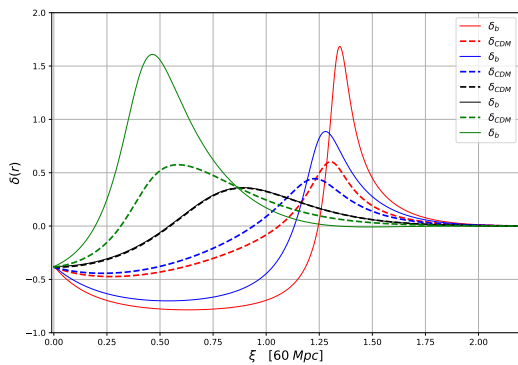


Fig. 2 Influence of the initial baryon peculiar velocity on voids and wall formation. Baryon and CDM density contrasts ($\delta_{(i)} = \rho_{(i)}/\bar{\rho}_{(i)} - 1$, where $\bar{\rho}_{(i)}$ is the value of $\rho_{(i)}$ in the background and $i = DM, B$) are depicted by dashed and solid lines, respectively, for different initial peculiar velocity profiles: all of them Gaussian functions with different amplitude (V_{peak} in Fig. 1) set initially at $z = 23$. The red lines stand for $V_{\text{peak}} \sim 7 \times 10^{-3}$, the blue lines for $V_{\text{peak}} \sim 5 \times 10^{-3}$ and the green ones for $V_{\text{peak}} \sim -2.6 \times 10^{-3}$. As a reference, we have provided the case without a relative velocity (LTB model), denoted by a black line. Note that the solution displayed by the solid blue curve includes a baryonic matter shell of width ~ 10 Mpc and density contrast of the order the unity and peculiar velocity of ~ 500 km/sec with respect to the CDM comoving frame. This configuration is roughly comparable with the dynamics of our local group, which has similar size and density contrast and a dipole velocity of ~ 600 km/s associated with its local motion with respect to the CMB frame [82].

where in order to derive eq. (25) we have used the fact that $V \ll 1$ (but its derivatives need not be small) and $\chi \equiv Y_{,r}$. Hence, the difference in the local expansion due to a change of frame can be expressed as follows,

$$3(H_B - H_{DM}) \simeq \left(\frac{2\chi}{Y} - \frac{B_{,r}}{B} \right) \frac{V}{B^2} + \frac{V_{,r}}{B^2} + V\dot{V}. \quad (26)$$

Figure 4 shows the difference between the two expansions H_B and H_{DM} at $z = 0$ for the solutions whose density contrast are depicted with red and blue lines in Fig. 2, corresponding to V_{peak} equal to 7×10^{-3} (red lines) and 5×10^{-3} (blue lines). Note that this difference can be of the order of km/(sMpc), around the maximum of the baryonic matter

density (even larger differences are expected at times close to virialization). This estimation is roughly that of the discrepancy between the values of H_0 reported by CMB and SNe observations [81, 85, 86], thus suggesting that considering a relative velocity between baryons and CDM may provide interesting clues to understand this issue (though this task lies beyond the scope of the present work).

3.4 The baryon–CDM relative velocity

Since for the baryon–CDM mixture the radial component of the relative velocity, as defined in Eq. (21), can be determined from the algebraic relation

$$V = Q_B/\rho_B, \quad (27)$$

with Q_B and ρ_B given by Eq. (22d)–(22e), its evolution equation is

$$\begin{aligned} \dot{V} &= (H - 2\Sigma) \frac{V^3}{B^2} + \frac{B_{,r}}{B^3} V^2 - \frac{V_{,r}}{B^2} V \\ &= \left(\frac{H - 2\Sigma}{B^2} \right) V^3 - \left(\frac{V^2}{2B^2} \right)_{,r}. \end{aligned} \quad (28)$$

where we used (20b), (20c) and $A \equiv 0$. In order to relate this equation to the well-studied perturbative case, we drop the term of order of V^3 to obtain,

$$\dot{V} \approx - \left(\frac{V^2}{2B^2} \right)_{,r}, \quad (29)$$

which shows the connection between the time evolution of the relative velocity and the radial gradients of the velocity and the metric function B that generalizes the background scale factor. In a quasi-homogeneous perturbative regime $B \sim a(t, r)r$ and thus $B_{,r} > 0$ should hold, while $V_{,r} > 0$ should also hold because relative velocities increase from the center onwards as r increases. Therefore the derivative of $(V^2)/(2B^2)$ should be positive and thus the right-hand side of the equation above negative. As a consequence, $\dot{V} < 0$ holds and relative velocities dilute asymptotically during

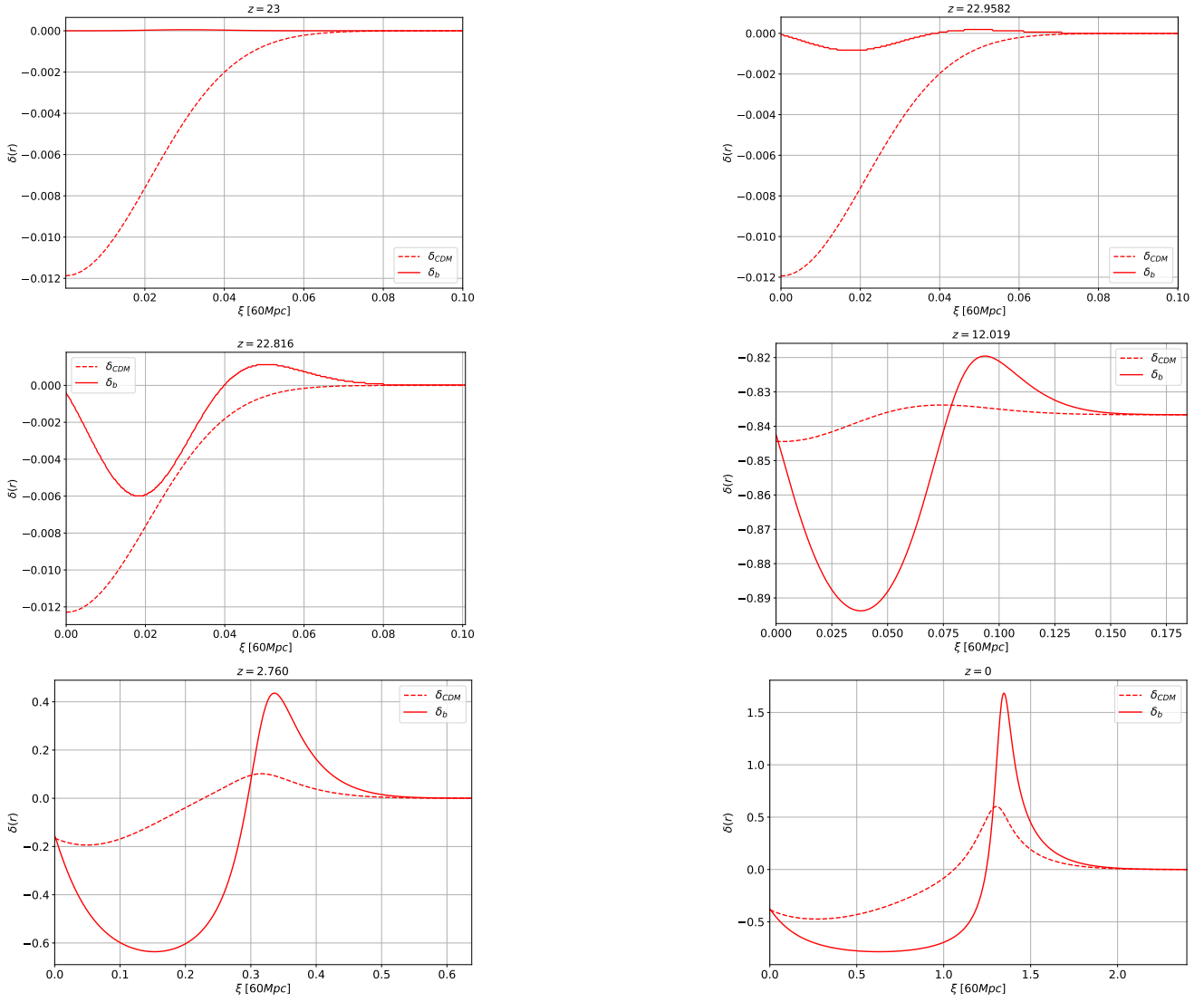


Fig. 3 The figure shows snapshots of the density contrast of each matter component at different redshifts for the solution depicted with red lines in Fig. 2.

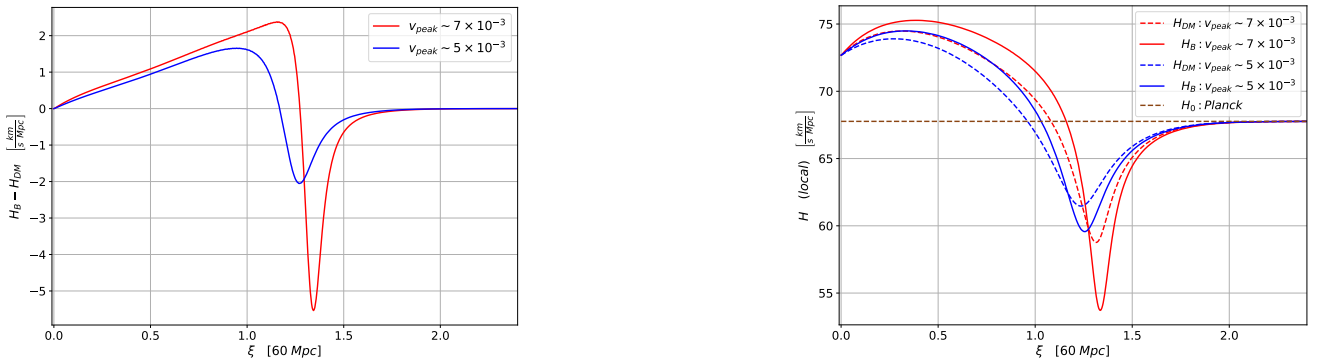


Fig. 4 Differences in the local expansion due to a change of frame. The left panel shows the difference between the two expansions at $z = 0$ (Eq. (26)) for two of the solutions depicted in Fig. 2, corresponding to V_{peak} equal to 7×10^{-3} (red lines) and 5×10^{-3} (blue lines). The right panel shows the local expansion of each component as computed from the solutions of the system (B.15) and Eq. (26).

cosmic expansion. However, this is not applicable to a non-perturbative regime where large gradients of the involved variables may occur and/or change signs, so that the relative velocity can be amplified by a local inhomogeneity.

We can obtain further information on the evolution of V by looking at a definition of peculiar velocity often used in a perturbative approach: the difference between the local Hubble flow relative to the Hubble flow of the background, which can be estimated as $v_{pec} = (H_{local} - H_{FLRW})Y$ [87]. Then, once again neglecting the highest power of V in Eq. (26), we get

$$\Delta v_{pec} = (H_b - H_{DM})Y \simeq \left(\frac{2\chi}{Y} - \frac{B_r}{B} \right) \frac{Y}{B^2} V + \frac{Y}{B^2} V_r, \quad (30)$$

which shows that such spatial velocity field is intrinsically related with the local homogeneities. At large scales (in a perturbative regime) this field evolves by approximately diluting as the inverse of the background scale factor, since in a regime approaching FLRW-like conditions our variables can be written as $B \sim a(r,t)$ and $Y \sim ra(r,t)$ (see e.g., [88] for a formal equivalence of LTB models with Cosmological Perturbation Theory in the linear regime). In an inhomogeneity, however, where the spatial gradients are not restricted to small values, the relative velocity and peculiar velocity must be found by a non-trivial evolution equation. In particular, for the numerical solutions showed in this section we found that the relative velocity decreases, but without following a trivial scaling law in the spatial region identified with the walls. Note that in such regions the gradients can be large and the local expansion is slower than the background expansion, in fact, in part it is locally collapsing.

4 Discussion and final remarks

We have considered the fully relativistic evolution of spherically symmetric cosmic voids made up of a mixture of two non-comoving dust components, identified as CDM and baryonic matter. Specifically, we looked at the effects of the baryon-CDM relative velocity on the void properties. We found that for baryons converging to the center of the void, as seen from the CDM frame, the final density profile shows an effective reduction on the size of the void (see Fig. 2). On the other hand, if the baryon component is receding from the centre, the void presents a deeper (baryonic) underdensity, and the walls manifest a larger density contrast as illustrated in Figs. 2 and 3.

The existence of a relative velocity between baryons and CDM leads to a difference in the expansion of each component. We find that small initial differences in velocities between two components (of order $7-5 \times 10^{-3}$) yield important differences in local expansion of the order of $\text{km}/(\text{sMpc})$, similar to the gap between local and CMB measurements of

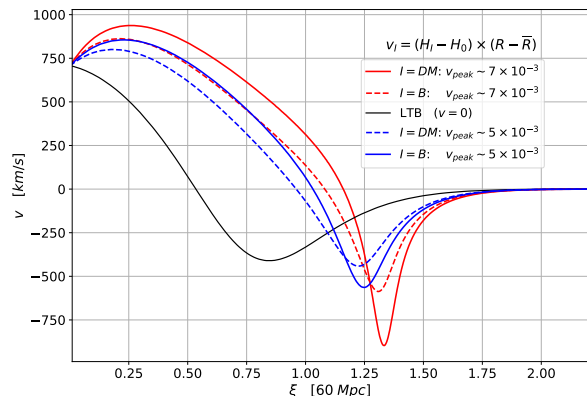


Fig. 5 Peculiar velocity of the void components with respect to the asymptotic background as defined in [87]. Note that the larger differences occur at the radii corresponding to the wall structure.

the expansion parameter H_0 [64, 81, 85, 86]. Indeed, this last result may be part of the effects missing in the usual single frame analysis of peculiar velocities and local expansion (e.g. curvature effects [67, 89], among others). Related to this, we find significant differences in the peculiar velocities of each component, defined as deviations from the asymptotic *background* (common) expansion, reached at large radii. Such differences could be interpreted as the velocity bias field, here evolved to non-linear stages. Fig. 5 shows that such bias manifests most prominently at the peak of the density contrast (walls of the void).

The spherical void model we work with is qualitatively analogous to earlier models [72–75]. As in these models, we obtain qualitatively analogous results that depict the expected streaming of baryons determined by the rapid void expansion, a characteristic also present in Newtonian models. However, the dynamical equations employed in the past are based on a numerical scheme constructed from the Misner–Sharp mass that is completely tied to spherical symmetry. As a contrast, the system of evolution equations and constraints here considered is based on covariant fluid–flow scalars that can be computed for any spacetime, regardless of the symmetry considerations.

Our approach to void dynamics could also represent an important improvement over the “silent models” of [67] that try to address this issue through “emergent” spatial curvature. Silent models (characterized by a non-rotating dust source with purely electric Weyl tensor) are theoretically handicapped by the conjecture stating that Einstein’s equations may not be integrable in general under the “silence” assumption [90, 91] (the models in [67] also neglect matching conditions among the different silent cells). By assuming dust sources with different (non-comoving) 4-velocities, the resulting models are based on similar physical assumptions but are no longer silent because of the non-trivial energy and momentum flux among the dust sources.

In conclusion, the fully relativistic evolution of baryons and CDM along different 4–velocity frames can provide important clues in understanding the observational tension in the estimation of the value of H_0 from local observations and through interpretation of the Planck data. A concrete example is furnished by the study of the Hubble flow in the non–spherical models examined in [64], which tries to understand this tension, but did not consider different 4–velocities for the baryon and CDM components. This work could be improved by allowing for a non–comoving baryon 4–velocity that would provide more degrees of freedom as we have done in this paper. Likewise the multiple fluid approach can provide important corrections to the usual study of the process of formation and growing of large–scale structure in the universe. Finally, we emphasize the fact that the system of evolution equations and constraints used in our numerical modeling has been constructed with covariant fluid flow variables, and thus it is readily applicable (under certain restrictions) to examine self–gravitating systems that are much less idealized than those under the assumption of spherical symmetry.

Acknowledgements The authors acknowledge support from research grants SEP–CONACYT 282569 and 239639. I.D.G. also acknowledges valuable discussions with S. Fromenteau.

Appendix A: Einstein’s field equations as a first order “1 + 3” system

Given a 4–velocity field, Einstein’s field equations are equivalent to a set of evolution and constraint equations involving the kinematic parameters Θ , \dot{u}^μ , $\sigma_{\mu\nu}$, $\omega_{\mu\nu}$ (expansion, 4–acceleration, shear and vorticity), the components of the energy momentum tensor ρ , p , $\Pi_{\mu\nu}$, q_μ (energy density, isotropic and anisotropic pressure, energy flux) projected by the 4–velocity, as well as the electric and magnetic parts of the Weyl tensor $E_{\mu\nu}$, $H_{\mu\nu}$. For spherical symmetry we have $\omega_{\mu\nu} = H_{\mu\nu} = 0$, hence the 1+3 system becomes the evolution equations

$$\dot{\rho} + 3(\rho + p)H + 2\dot{u}^\mu q_\mu + \tilde{\nabla}_\mu u^\mu + \pi_{\mu\nu}\sigma^{\mu\nu} = 0, \quad (\text{A.1})$$

$$3\dot{H} + 3H^2 + \frac{\kappa}{2}(\rho + 3p)\sigma_{\mu\nu}\pi^{\mu\nu} - \tilde{\nabla}_\mu \dot{u}^\mu - \dot{u}_\mu \dot{u}^\mu = 0, \quad (\text{A.2})$$

$$\dot{q}_{\langle\mu\rangle} + 4Hq_\mu + (\rho + p)\dot{u}_\mu + \tilde{\nabla}_\mu p + \tilde{\nabla}_\nu \pi_\mu^\nu + \pi_{\mu\nu}\dot{u}^\nu + \sigma_{\mu\nu}q^\nu = 0, \quad (\text{A.3})$$

$$\dot{\sigma}_{\langle\mu\nu\rangle} + 2H\sigma_{\mu\nu} + E_{\mu\nu} - \frac{\kappa}{2}\pi_{\mu\nu} - \tilde{\nabla}_{\langle\mu}\dot{u}_{\nu\rangle} + \sigma_{\nu\langle\mu}\dot{\sigma}_{\nu\rangle}^\nu - \dot{u}_{\langle\mu}\dot{u}_{\nu\rangle} = 0, \quad (\text{A.4})$$

$$\dot{E}_{\langle\mu\nu\rangle} + 3HE_{\mu\nu} + \kappa\dot{u}_{\langle\mu}q_{\nu\rangle} - 3\sigma_{\nu\langle\mu}E_{\nu\rangle}^\nu + \frac{\kappa}{2}\left[(\rho + p)\sigma_{\mu\nu} + \dot{\pi}_{\langle\mu\nu\rangle} + \frac{3}{4}H\pi_{\mu\nu} + \tilde{\nabla}_{\langle\mu}q_{\nu\rangle}\right] = 0, \quad (\text{A.5})$$

together with the constraints

$$\tilde{\nabla}_\nu \sigma_\mu^\nu - 2\tilde{\nabla}_\mu H + \kappa q_\mu = 0, \quad (\text{A.6})$$

$$\tilde{\nabla}_\nu E_\mu^\nu - \frac{\kappa}{3}\left(\tilde{\nabla}_\mu \rho - 3Hq_\mu - \frac{1}{2}\tilde{\nabla}_\nu \pi_\mu^\nu\right) - \frac{\kappa}{2}\sigma_{\mu\nu}q^\nu = 0, \quad (\text{A.7})$$

$$H^2 - \frac{\kappa}{3}\rho - \frac{1}{6}\sigma_{\mu\nu}\sigma^{\mu\nu} + \frac{1}{6}{}^{(3)}\mathcal{R} = 0, \quad (\text{A.8})$$

where the “dot” and “tilde” respectively denote the convective (projected with u^μ) derivative and spacelike gradients (projected orthogonal to u^μ), see (3), while indices enclosed by angle brackets $\langle\mu\nu\rangle$ denote the spacelike symmetric tracefree projection (see (10b)).

In order to apply the system (A.1)–(A.8) to the fluid mixture we need to substitute (14a)–(14d) for the total forms of ρ , p , $\pi_{\mu\nu}$ and q_μ , as well as the forms for the kinematic parameters and electric Weyl tensor in (4b) and (7).

Notice that the system (A.1)–(A.8) is not only valid for spherically symmetric spacetimes, but for Petrov type D spacetime ($H_{\mu\nu} = 0$) whose source is endowed with an irrotational fluid 4–velocity ($\omega_{\mu\nu} = 0$). The system can be readily extended to more general spacetimes. While it does not involve metric functions, information on these functions is very useful for the numerical solution of the constraints.

Appendix B: The dimensionless system of PDEs

For the CDM–baryon problem where both species are assumed to be strictly dust fluids ($p \equiv 0$), Eqs. (17b) and (20a) imply that,

$$A \equiv 0, \quad \text{and} \quad N = 1, \quad (\text{B.9})$$

with A defined in (5). Then, redefining the “dot” derivative:

$$\hat{\Phi} = \frac{\dot{\Phi}}{H_*} = \frac{1}{H_*}u^\mu \nabla_\mu \Phi = \frac{\Phi_{,t}}{H_*N} = \frac{\Phi_{,t}}{H_*}, \quad (\text{B.10})$$

where H_* is a constant with inverse–length units sets equal to the initial background Hubble constant.

We introduce the following dimensionless parameters and functions:

$$Y = l_*\mathcal{Y}, \quad r = l_*\xi, \quad \alpha = 1/(H_*l_*), \quad (\text{B.11})$$

$$\mathcal{S} = \frac{\Sigma}{H_*}, \quad \mathcal{H} = \frac{H}{H_*}, \quad \mathcal{W} = \frac{W}{H_*^2}, \quad \chi = \mathcal{Y}_{,\xi}, \quad (\text{B.12})$$

$$\mu = \frac{\kappa\rho}{3H_*^2}, \quad \text{p} = \frac{\kappa p}{3H_*^2}, \quad (\text{B.13})$$

$$\mathcal{M} = \frac{\kappa M}{3H_*^2}, \quad \mathcal{Q} = \frac{\kappa Q}{3H_*^2}, \quad \mathcal{P} = \frac{\kappa \Pi}{3H_*^2}, \quad (\text{B.14})$$

with the characteristic length $l_* \sim 60$ Mpc. From substituting $0 \rightarrow \text{DM}$, $i \rightarrow \text{B}$, and the above–defined dimensionless functions in the system (16), we obtain the desired dimensionless

system of PDEs governing the dynamics of a 2–dust–fluid mixture:

$$\hat{\mathcal{Y}} = \mathcal{Y} (\mathcal{H} + \mathcal{S}), \quad (\text{B.15a})$$

$$\hat{\chi} = -2\chi\mathcal{S} + \chi\mathcal{H} + \frac{3}{2\alpha}\mathcal{Q}\mathcal{Y}, \quad (\text{B.15b})$$

$$\hat{B} = B(\mathcal{H} - 2\mathcal{S}), \quad (\text{B.15c})$$

$$\hat{\mathcal{H}} = -\mathcal{H}^2 - 2\mathcal{S}^2 - \frac{1}{2}(\mu + 3p), \quad (\text{B.15d})$$

$$\hat{\mathcal{S}} = \mathcal{S}^2 - 2\mathcal{H}\mathcal{S} + \frac{3}{2}\mathcal{P} - \mathcal{W}, \quad (\text{B.15e})$$

$$\hat{\mu}_{\text{DM}} = -3\mu_{\text{DM}}\mathcal{H}, \quad (\text{B.15f})$$

$$\hat{\mu}_{\text{B}} = -3(\mu_{\text{B}} + p)\mathcal{H} - 6\mathcal{P}\mathcal{S} - \frac{2\alpha\mathcal{Q}\chi}{\mathcal{Y}B^2} - \frac{\alpha\mathcal{Q}_{,\xi}}{B^2} + \frac{\alpha\mathcal{Q}B_{,\xi}}{B^3}, \quad (\text{B.15g})$$

$$\hat{\mathcal{Q}} = -3\mathcal{H}\mathcal{Q} - \alpha p_{,\xi} + 2\alpha\mathcal{P}_{,\xi} + \frac{6\alpha\mathcal{P}\chi}{\mathcal{Y}}, \quad (\text{B.15h})$$

where

$$\mu_{\text{B}} = \gamma^2\mu_{\text{B}}^*, \quad p \equiv p_{\text{B}} = \frac{1}{3}\gamma^2v^2\mu_{\text{B}}^*, \quad (\text{B.15i})$$

$$\mathcal{Q} \equiv \mathcal{Q}_{\text{B}} = \gamma^2\mu_{\text{B}}^*V, \quad \mathcal{P} \equiv \mathcal{P}_{\text{B}} = \frac{1}{3}\gamma^2\mu_{\text{B}}^*v^2, \quad (\text{B.15j})$$

$$\mu = \mu_{\text{DM}} + \mu_{\text{B}}. \quad (\text{B.15k})$$

At each time the velocity and intrinsic density of the second (non–comoving) dust is determined by:

$$V = \frac{\mathcal{Q}}{\mu_{\text{B}}}, \quad \text{and} \quad \mu_{\text{B}}^* = \frac{\mu_{\text{B}}^2 - \mathcal{Q}_{\text{B}}^2}{\mu_{\text{B}}}. \quad (\text{B.15l})$$

The system is complemented by the following constraints

$$\mathcal{H}^2 = \mu - k + \mathcal{S}^2, \quad \text{with} \quad k = \frac{\mathcal{K}}{H_*^2}, \quad (\text{B.15m})$$

$$\mathcal{W} = -\frac{\mu}{2} + \frac{\mathcal{M}}{\mathcal{Y}^3} - \frac{3\mathcal{P}}{2}, \quad (\text{B.15n})$$

where,

$$\mathcal{M} = \frac{1}{2}\mathcal{Y} \left(\mathcal{Y}^2(\mathcal{S} + \mathcal{H})^2 - \frac{\alpha^2\chi^2}{B^2} + 1 \right). \quad (\text{B.15o})$$

On the other hand, the equation (16f) (redundant) results,

$$\begin{aligned} \hat{\mathcal{W}} + \frac{3}{2}\hat{\mathcal{P}} &= -3(\mathcal{H} + \mathcal{S})\mathcal{W} - \frac{3}{2}(\mu + p)\mathcal{S} \\ &- \frac{3}{2}(\mathcal{H} - \mathcal{S})\mathcal{P} - \frac{\alpha B_{,\xi}\mathcal{Q}}{2B^3} + \frac{\alpha\mathcal{Q}_{,\xi}}{2B^2} - \frac{\alpha\chi\mathcal{Q}}{2B^2\mathcal{Y}}, \end{aligned} \quad (\text{B.16})$$

We employed the Method of Lines to integrate this system of PDEs. Proceeding in this way the PDEs were discretized along the radial variable, setting 1000 grid points within the interval $r/l_* \in [0, 0.2]$. The resulting set of ordinary differential equations was integrated using an adaptive step–size Runge–Kutta of 4(5)–th order.

Appendix C: LTB limit

The LTB model is a general inhomogeneous spherically symmetric solution of the Einstein’s equations for a single irrotational dust fluid as source $T^{\mu\nu} = \rho u^\mu u^\nu$. The time–synchronous metric can be cast as follows [92],

$$ds^2 = -dt^2 + \frac{R_{,r}^2(r,t)}{1+2E(r)}dr^2 + R^2(r,t)(d\theta^2 + \sin^2(\theta)d\phi^2). \quad (\text{C.17})$$

For a comoving 4–velocity $u^\mu = \delta_t^\mu$ the field equations reduce to:

$$\dot{R}^2 = \frac{2M}{R} + 2E, \quad \text{and} \quad M_{,r} = \frac{\kappa}{2}\rho R^2 R_{,r}, \quad (\text{C.18})$$

Following a similar approach to that used in the main text, we rewrite the Einstein’s equations in terms of covariant objects associated with the 4–velocity and the energy–momentum and projection tensors, which leads to,

$$\dot{H} = -H^2 - \frac{\kappa}{6}\rho - 2\Sigma^2, \quad (\text{C.19a})$$

$$\dot{\rho} = -3\rho H, \quad (\text{C.19b})$$

$$\dot{\Sigma} = -2H\Sigma + \Sigma^2 - \mathcal{W}, \quad (\text{C.19c})$$

$$\dot{\mathcal{W}} = -\frac{\kappa}{2}\rho\Sigma - 3\mathcal{W}(H + \Sigma), \quad (\text{C.19d})$$

together with the constraint (among others not listed here)

$$H^2 = \frac{\kappa}{3}\rho - \mathcal{K} + \Sigma^2, \quad (\text{C.19e})$$

where the expansion scalar, the eigenvalues of the shear and magnetic Weyl tensors as well as the spatial curvature take the simple form:

$$3H = \frac{2\dot{R}}{R} + \frac{\dot{R}'}{R'}, \quad \Sigma = -\frac{1}{3} \left(\frac{\dot{R}_{,r}}{R_{,r}} - \frac{\dot{R}}{R} \right), \quad (\text{C.20})$$

$$\mathcal{W} = -\frac{M}{R^3} + \frac{\kappa}{6}\rho, \quad \mathcal{K} = -\frac{4(ER)_{,r}}{6R^2R_{,r}}. \quad (\text{C.21})$$

These previous equations are recovered by specializing the system (16)–(19) (or its particular case (B.15)) to the single comoving fluid case. This can be checked by making the following substitutions:

$$v \rightarrow 0, \quad N \rightarrow 1, \quad Y \rightarrow R, \quad B \rightarrow \frac{R'}{1+2E}, \quad 2E \rightarrow -K. \quad (\text{C.22})$$

References

1. Noam I Libeskind, Rien Van De Weygaert, Marius Cautun, Bridget Falck, Elmo Tempel, Tom Abel, Mehmet Alpaslan, Miguel A Aragón-Calvo, Jaime E Forero-Romero, Roberto Gonzalez, et al. Tracing the cosmic web. *Monthly Notices of the Royal Astronomical Society*, 473(1):1195–1217, 2018.

2. PJE Peebles. The void phenomenon. *The Astrophysical Journal*, 557(2):495, 2001.
3. Yasmin Friedmann and Tsvi Piran. A model of void formation. *The Astrophysical Journal*, 548(1):1, 2001.
4. Rien van de Weygaert and Erwin Platen. Cosmic voids: structure, dynamics and galaxies. In *International Journal of Modern Physics: Conference Series*, volume 1, pages 41–66. World Scientific, 2011.
5. Rien van de Weygaert. Voids and the cosmic web: cosmic depression & spatial complexity. *Proceedings of the International Astronomical Union*, 11(S308):493–523, 2014.
6. PM Sutter, Pascal Elahi, Bridget Falck, Julian Onions, Nico Hamaus, Alexander Knebe, Chaichalit Srisawat, and Aurel Schneider. The life and death of cosmic voids. *Monthly Notices of the Royal Astronomical Society*, 445(2):1235–1244, 2014.
7. Nico Hamaus, PM Sutter, and Benjamin D Wandelt. Modeling cosmic void statistics. *Proceedings of the International Astronomical Union*, 11(S308):538–541, 2014.
8. Summary of catalogues. <http://www.cosmicvoids.net>.
9. Lizhi Xie, Liang Gao, and Qi Guo. The local void: for or against λ cdm? *Monthly Notices of the Royal Astronomical Society*, 441(2):933–938, 2014.
10. Nico Hamaus, Alice Pisani, Paul M Sutter, Guilhem Lavaux, Stéphanie Escoffier, Benjamin D Wandelt, and Jochen Weller. Constraints on cosmology and gravity from the dynamics of voids. *Physical review letters*, 117(9):091302, 2016.
11. Seshadri Nadathur. Testing cosmology with a catalogue of voids in the boss galaxy surveys. *Monthly Notices of the Royal Astronomical Society*, 461(1):358–370, 2016.
12. Jounghun Lee and Daeseong Park. Constraining the dark energy equation of state with cosmic voids. *The Astrophysical Journal Letters*, 696(1):L10, 2009.
13. Stephon Alexander, Tirthabir Biswas, Alessio Notari, and Deepak Vaid. Local void vs dark energy: confrontation with wmap and type ia supernovae. *Journal of Cosmology and Astroparticle Physics*, 2009(09):025, 2009.
14. Rahul Biswas, Esfandiar Alizadeh, and Benjamin D Wandelt. Voids as a precision probe of dark energy. *Physical Review D*, 82(2):023002, 2010.
15. Arnaud de Lavallaz and Malcolm Fairbairn. Effects of voids on the reconstruction of the equation of state of dark energy. *Physical Review D*, 84(8):083005, 2011.
16. EG Patrick Bos, Rien van de Weygaert, Klaus Dolag, and Valeria Pettorino. The darkness that shaped the void: dark energy and cosmic voids. *Monthly Notices of the Royal Astronomical Society*, 426(1):440–461, 2012.
17. Boudewijn F Roukema. Dark energy with rigid voids versus relativistic voids alone. *International Journal of Modern Physics D*, 22(12):1341018, 2013.
18. PM Sutter, Edoardo Carlesi, Benjamin D Wandelt, and Alexander Knebe. On the observability of coupled dark energy with cosmic voids. *Monthly Notices of the Royal Astronomical Society: Letters*, 446(1):L1–L5, 2014.
19. Alice Pisani, PM Sutter, Nico Hamaus, Esfandiar Alizadeh, Rahul Biswas, Benjamin D Wandelt, and Christopher M Hirata. Counting voids to probe dark energy. *Physical Review D*, 92(8):083531, 2015.
20. Eromanga Adermann, Pascal J Elahi, Geraint F Lewis, and Chris Power. Cosmic voids in evolving dark sector cosmologies: the high-redshift universe. *Monthly Notices of the Royal Astronomical Society*, 479(4):4861–4877, 2018.
21. G Pollina, N Hamaus, K Paech, K Dolag, J Weller, C Sánchez, ES Rykoff, B Jain, TMC Abbott, S Allam, et al. On the relative bias of void tracers in the dark energy survey. *arXiv preprint arXiv:1806.06860*, 2018.
22. Nico Hamaus, PM Sutter, Guilhem Lavaux, and Benjamin D Wandelt. Probing cosmology and gravity with redshift-space distortions around voids. *Journal of Cosmology and Astroparticle Physics*, 2015(11):036, 2015.
23. Ixandra Achitouv. Improved model of redshift-space distortions around voids: Application to quintessence dark energy. *Physical Review D*, 96(8):083506, 2017.
24. Yue Nan and Kazuhiro Yamamoto. Gravitational redshift in void-galaxy cross-correlation function in redshift space. *arXiv preprint arXiv:1805.05708*, 2018.
25. Kei-ichi Maeda, Nobuyuki Sakai, and Roland Triay. Dynamics of voids and their shapes in redshift space. *Journal of Cosmology and Astroparticle Physics*, 2011(08):026, 2011.
26. Yan-Chuan Cai, Mark C Neyrinck, Istvan Szapudi, Shaun Cole, and Carlos S Frenk. A possible cold imprint of voids on the microwave background radiation. *The Astrophysical Journal*, 786(2):110, 2014.
27. Kaiki Taro Inoue and Joseph Silk. Local voids as the origin of large-angle cosmic microwave background anomalies. i. *The Astrophysical Journal*, 648(1):23, 2006.
28. Seshadri Nadathur and Subir Sarkar. Reconciling the local void with the cmb. *Physical Review D*, 83(6):063506, 2011.
29. Teeraparb Chantavat, Utane Sawangwit, Paul M Sutter, and Benjamin D Wandelt. Cosmological parameter constraints from cmb lensing with cosmic voids. *Physical Review D*, 93(4):043523, 2016.
30. Yan-Chuan Cai, Mark Neyrinck, Qingqing Mao, John A Peacock, Istvan Szapudi, and Andreas A Berlind. The lensing and temperature imprints of voids on the cosmic microwave background. *Monthly Notices of the Royal Astronomical Society*, 466(3):3364–3375, 2016.

31. Cheng Zhao, Chia-Hsun Chuang, Yu Liang, Francisco-Shu Kitaura, Mariana Vargas-Magaña, Charling Tao, Marcos Pellejero-Ibanez, and Gustavo Yepes. Improving baryon acoustic oscillation measurement with the combination of cosmic voids and galaxies. *arXiv preprint arXiv:1802.03990*, 2018.
32. Nico Hamaus, Alice Pisani, P. M. Sutter, Guilhem Lavaux, Stéphanie Escoffier, Benjamin D. Wandelt, and Jochen Weller. Constraints on cosmology and gravity from the dynamics of voids. *Phys. Rev. Lett.*, 117:091302, Aug 2016. doi: 10.1103/PhysRevLett.117.091302. URL <https://link.aps.org/doi/10.1103/PhysRevLett.117.091302>.
33. Paul Zivick, PM Sutter, Benjamin D Wandelt, Baojiu Li, and Tsz Yan Lam. Using cosmic voids to distinguish $f(r)$ gravity in future galaxy surveys. *Monthly Notices of the Royal Astronomical Society*, 451(4):4215–4222, 2015.
34. Douglas Spolyar, Martin Sahlén, and Joe Silk. Topology and dark energy: testing gravity in voids. *Physical review letters*, 111(24):241103, 2013.
35. Rodrigo Voivodic, Marcos Lima, Claudio Llinares, and David F Mota. Modeling void abundance in modified gravity. *Physical Review D*, 95(2):024018, 2017.
36. Martin Sahlén and Joseph Silk. Cluster-void degeneracy breaking: Modified gravity in the balance. *Physical Review D*, 97(10):103504, 2018.
37. Joseph Clampitt, Yan-Chuan Cai, and Baojiu Li. Voids in modified gravity: excursion set predictions. *Monthly Notices of the Royal Astronomical Society*, 431(1):749–766, 2013.
38. R Brent Tully. Our cmb motion: The role of the local void. In *ASP Conf. Ser.*, volume 379, page 24, 2006.
39. JI Davies and MJ Dtsney. The local void is really empty. *Dark Galaxies and Lost Baryons (IAU S244)*, 244:146, 2008.
40. R Brent Tully, Edward J Shaya, Igor D Karachentsev, Hélène M Courtois, Dale D Kocevski, Luca Rizzi, and Alan Peel. Our peculiar motion away from the local void. *The Astrophysical Journal*, 676(1):184, 2008.
41. Guilhem Lavaux. Dynamics of the local universe: cosmic velocity flows and voids. In *AIP Conference Proceedings*, volume 1241, pages 1001–1010. AIP, 2010.
42. OG Nasonova and ID Karachentsev. Kinematics of the local cosmic void. *Astrophysics*, 54(1):1–14, 2011.
43. Marcelo Lares, Heliana E Luparello, Victoria Maldonado, Andrés N Ruiz, Dante J Paz, Laura Ceccarelli, and Diego Garcia Lambas. Voids and superstructures: correlations and induced large-scale velocity flows. *Monthly Notices of the Royal Astronomical Society*, 470(1):85–94, 2017.
44. Kyungjin Ahn and Britton D Smith. Formation of first galaxies inside density peaks and voids under the influence of dark matter-baryon streaming velocity, i: Initial condition and simulation scheme. *arXiv preprint arXiv:1807.04063*, 2018.
45. Roberto A Sussman and Julien Larena. Gravitational entropy of local cosmic voids. *Classical and Quantum Gravity*, 32(16):165012, 2015.
46. Priti Mishra and Tejinder P Singh. Thermodynamics and lemaître-tolman-bondi void models. *Physical Review D*, 89(12):123007, 2014.
47. Vasilij Demchenko, Yan-Chuan Cai, Catherine Heymans, and John A Peacock. Testing the spherical evolution of cosmic voids. *Monthly Notices of the Royal Astronomical Society*, 463(1):512–519, 2016.
48. Nico Hamaus, PM Sutter, and Benjamin D Wandelt. Universal density profile for cosmic voids. *Physical review letters*, 112(25):251302, 2014.
49. E Ricciardelli, V Quilis, and J Varela. On the universality of void density profiles. *Monthly Notices of the Royal Astronomical Society*, 440(1):601–609, 2014.
50. V. Icke. Voids and filaments. *Monthly Notices of the Royal Astronomical Society*, 206:1P–3P, January 1984. doi: 10.1093/mnras/206.1.1P.
51. Humitaka Sato and Kei-ichi Maeda. The expansion law of the void in the expanding universe. *Progress of Theoretical Physics*, 70(1):119–127, 1983.
52. Radosław Wojtak, Devon Powell, and Tom Abel. Voids in cosmological simulations over cosmic time. *Monthly Notices of the Royal Astronomical Society*, 458(4):4431–4442, 2016.
53. Paul de Fromont and Jean-Michel Alimi. Reconstructing matter profiles of spherically compensated cosmic regions in Λ CDM cosmology. *Monthly Notices of the Royal Astronomical Society*, 473:5177–5194, February 2018. doi: 10.1093/mnras/stx2677.
54. Krzysztof Bolejko, Andrzej Krasinski, and Charles Hellaby. Formation of voids in the universe within the lemaître–tolman model. *Monthly Notices of the Royal Astronomical Society*, 362(1):213–228, 2005.
55. Krzysztof Bolejko. Radiation in the process of the formation of voids. *Monthly Notices of the Royal Astronomical Society*, 370(2):924–932, 2006.
56. K. Bolejko, A. Krasinski, C. Hellaby, and M.-N. Célérier. Cambridge University Press, October 2009.
57. A Iribarrem, P Andreani, S February, C Gruppioni, AR Lopes, MB Ribeiro, and WR Stoeger. Relativistic cosmology number densities in void-lemaître-tolman-bondi models. *Astronomy & Astrophysics*, 563:A20, 2014.
58. K. Bolejko and R. A. Sussman. Cosmic spherical void via coarse-graining and averaging non-spherical structures. *Physics Letters B*, 697:265–270, March 2011. doi: 10.1016/j.physletb.2011.02.007.

59. Roberto A Sussman and I Delgado Gaspar. Multiple nonspherical structures from the extrema of szekeres scalars. *Physical Review D*, 92(8):083533, 2015.
60. Roberto A. Sussman, I. Delgado Gaspar, and Juan Carlos Hidalgo. Coarse-grained description of cosmic structure from Szekeres models. *JCAP*, 1603(03):012, 2016. doi: 10.1088/1475-7516/2016/06/E03,10.1088/1475-7516/2016/03/012. [Erratum: JCAP1606,no.06,E03(2016)].
61. Roberto A Sussman, Juan Carlos Hidalgo, Ismael Delgado Gaspar, and Gabriel Germán. Nonspherical szekeres models in the language of cosmological perturbations. *Physical Review D*, 95(6):064033, 2017.
62. Vassilios Mewes, Yosef Zlochower, Manuela Campanelli, Ian Ruchlin, Zachariah B Etienne, and Thomas W Baumgarte. Numerical relativity in spherical coordinates with the einstein toolkit. *Physical Review D*, 97(8):084059, 2018.
63. Hayley J Macpherson, Paul D Lasky, and Daniel J Price. Inhomogeneous cosmology with numerical relativity. *Physical Review D*, 95(6):064028, 2017.
64. Hayley J Macpherson, Paul D Lasky, and Daniel J Price. The trouble with hubble: Local versus global expansion rates in inhomogeneous cosmological simulations with numerical relativity. *The Astrophysical Journal Letters*, 865(1):L4, 2018.
65. Eloisa Bentivegna and Marco Bruni. Effects of nonlinear inhomogeneity on the cosmic expansion with numerical relativity. *Physical review letters*, 116(25):251302, 2016.
66. David Daverio, Yves Dirian, and Ermis Mitsou. A numerical relativity scheme for cosmological simulations. *Classical and Quantum Gravity*, 34(23):237001, 2017.
67. Krzysztof Bolejko. Relativistic numerical cosmology with silent universes. *Classical and Quantum Gravity*, 35(2):024003, 2017.
68. José M Torres, Miguel Alcubierre, Alberto Diez-Tejedor, and Darío Núñez. Cosmological nonlinear structure formation in full general relativity. *Physical Review D*, 90(12):123002, 2014.
69. Paul D Lasky and Anthony WC Lun. Spherically symmetric gravitational collapse of general fluids. *Physical Review D*, 75(2):024031, 2007.
70. Paul D Lasky and Anthony WC Lun. Generalized lemaitre-tolman-bondi solutions with pressure. *Physical Review D*, 74(8):084013, 2006.
71. Woei Chet Lim, Marco Regis, and Chris Clarkson. Spherically symmetric cosmological spacetimes with dust and radiation?numerical implementation. *Journal of Cosmology and Astroparticle Physics*, 2013(10):010, 2013.
72. Do Young Kim, Anthony N Lasenby, and Michael P Hobson. An alternative approach to modelling a cosmic void and its effect on the cosmic microwave background. *arXiv preprint arXiv:1804.02927*, 2018.
73. M Tsizh and B Novosyadlyj. Evolution of density and velocity profiles of matter in large voids. *Advances in Astronomy and Space Physics*, 6:28–33, 2016.
74. Bohdan Novosyadlyj, Maksym Tsizh, and Yuriy Kulinich. Evolution of density and velocity profiles of dark matter and dark energy in spherical voids. *Monthly Notices of the Royal Astronomical Society*, page stw2767, 2016.
75. Valerio Marra and Mikko Paakkonen. Exact spherically-symmetric inhomogeneous model with n perfect fluids. *JCAP*, 1201:025, 2012. doi: 10.1088/1475-7516/2012/01/025.
76. George FR Ellis and Henk Van Elst. Cosmological models. In *Theoretical and Observational Cosmology*, pages 1–116. Springer, 1999.
77. Christos G. Tsagas, Anthony Challinor, and Roy Maartens. Relativistic cosmology and large-scale structure. *Phys. Rept.*, 465:61–147, 2008. doi: 10.1016/j.physrep.2008.03.003.
78. George FR Ellis, Roy Maartens, and Malcolm AH MacCallum. *Relativistic cosmology*. Cambridge University Press, 2012.
79. Roy Maartens, Tim Gebbie, and George FR Ellis. Cosmic microwave background anisotropies: Nonlinear dynamics. *Physical Review D*, 59(8):083506, 1999.
80. K. Bolejko, M.-N. Célérier, and A. Krasinski. Inhomogeneous cosmological models: exact solutions and their applications. *Classical and Quantum Gravity*, 28(16):164002, August 2011. doi: 10.1088/0264-9381/28/16/164002.
81. Peter AR Ade, N Aghanim, M Arnaud, M Ashdown, J Aumont, C Baccigalupi, AJ Banday, RB Barreiro, JG Bartlett, N Bartolo, et al. Planck 2015 results-xiii. cosmological parameters. *Astronomy & Astrophysics*, 594:A13, 2016.
82. A. Kogut et al. Dipole anisotropy in the COBE DMR first year sky maps. *Astrophys. J.*, 419:1, 1993. doi: 10.1086/173453.
83. J. Binney and S. Tremaine. *Galactic Dynamics: Second Edition*. Princeton University Press, 2008.
84. Ismael Delgado Gaspar, Juan Carlos Hidalgo, Roberto A. Sussman, and Israel Quiros. Black hole formation from the gravitational collapse of a nonspherical network of structures. *Phys. Rev. D*, 97:104029, May 2018. doi: 10.1103/PhysRevD.97.104029. URL <https://link.aps.org/doi/10.1103/PhysRevD.97.104029>.
85. Adam G. Riess, Lucas M. Macri, Samantha L. Hoffmann, Dan Scolnic, Stefano Casertano, Alexei V. Filippenko, Brad E. Tucker, Mark J. Reid, David O. Jones, Jeffrey M. Silverman, Ryan Chornock, Peter Challis,

- Wenlong Yuan, Peter J. Brown, and Ryan J. Foley. A 2.4 determination of the local value of the hubble constant. *The Astrophysical Journal*, 826(1):56, 2016. URL <http://stacks.iop.org/0004-637X/826/i=1/a=56>.
86. Wendy L Freedman. Cosmology at a crossroads. *Nat. Astron.*, 1:0121, 2017.
87. Krzysztof Bolejko and Charles Hellaby. The great attractor and the shapley concentration. *General Relativity and Gravitation*, 40(8):1771–1790, Aug 2008. ISSN 1572-9532. doi: 10.1007/s10714-007-0573-5. URL <https://doi.org/10.1007/s10714-007-0573-5>.
88. Roberto A. Sussman, Juan Carlos Hidalgo, Peter K. S. Dunsby, and Gabriel German. Spherical dust fluctuations: The exact versus the perturbative approach. *Phys. Rev.*, D91(6):063512, 2015. doi: 10.1103/PhysRevD.91.063512.
89. Krzysztof Bolejko. Emerging spatial curvature can resolve the tension between high-redshift cmb and low-redshift distance ladder measurements of the hubble constant. *Phys. Rev. D*, 97:103529, May 2018. doi: 10.1103/PhysRevD.97.103529. URL <https://link.aps.org/doi/10.1103/PhysRevD.97.103529>.
90. Henk Van Elst, Claes Uggla, William M Lesame, George FR Ellis, and Roy Maartens. Integrability of irrotational silent cosmological models. *Classical and Quantum Gravity*, 14(5):1151, 1997.
91. Carlos F Sopuerta. New study of silent universes. *Physical Review D*, 55(10):5936, 1997.
92. Roberto A Sussman. Weighed scalar averaging in ltb dust models: part i. statistical fluctuations and gravitational entropy. *Classical and Quantum Gravity*, 30(6):065015, 2013.